7R.3 QUANTITATIVE INTERPRETATION OF PRECIPITATION RADAR MEASUREMENTS AT VHF BAND

Edwin F. Campos [1*], Frédéric Fabry[1], and Wayne Hocking[2]
[1]*Department of Atmospheric and Oceanic Sciences, McGill University, Montreal, Quebec, Canada*
[2]*Department of Physics, University of Western Ontario, London, Ontario, Canada*

1. INTRODUCTION

Quantitative interpretation of precipitation measurements in the VHF band implies the extraction of the precipitation signal out of the full power spectra, as well as the proper conversion of this signal into reflectivity factors. In addition, a proper relationship between radar received powers and scatterers cross-sections (i.e., a radar equation) is required. We will explore this aspects here, utilizing simultaneous observations of co-located vertically pointing radars, operating in the VHF and X bands, as well as drop-size-distribution measurements at ground.

2. METHODS

2.1. The radar equation

Standard forms for this equation assume an average scatterer cross-section per unit volume (or radar reflectivity) that is constant within the sampling volume of a given range gate. Under these conditions, the radar equation valid for vertically pointing radars is given by the following expression:

$$P_r = \frac{A_e\, P_{Tx}\, e_a\, D_{\max}\, \bar{\eta}}{16\pi^2} \int_{r=H}^{H+L/2} \int_{f=0}^{2\pi} \int_{q=0}^{\pi/2} \frac{[F(q,f)]^2 \sin q}{r^2}\, dq\, df\, dr \quad ;(1)$$

where P_r is the received power (in Watts), A_e is the radar antenna effective area (in m^2), P_{Tx} is the transmitter power (in Watts), e_a is the antenna efficiency, F is the antenna pattern (or polar diagram), D_{max} is the antenna-pattern maximum directivity, $\bar{\eta}$ is the radar reflectivity (in m^{-1}), r is the range (in meters), L is the transmitted pulse length (in meters), H is the lower height within the range gate (in meters), f is the azimuth angle, and q is the zenith angle.

Equation (1) is appropriate when dealing with radars that have a narrow transmitted beam and high range resolution. However, this relation may not be valid for radars with antenna pattern having significant side lobes (e.g., the McGill VHF radar). The reason is that the radar will receive additional power from scatterers located at the same distance but in a different direction than the main-beam range-gate. Therefore, it is the following radar equation the one to be solved:

$$P_r = \frac{A_e\, P_{Tx}\, e_a\, D_{\max}}{16\pi^2} \int_{r=H}^{H+L/2} \int_{f=0}^{2\pi} \int_{q=0}^{\pi/2} \frac{\eta(r,q,f)[F(q,f)]^2 \sin q}{r^2}\, dq\, df\, dr \quad .(2)$$

This project will then explore the effect of using equation (2), instead of (1), when computing profiles of equivalent reflectivity factor. The next section will describe the method used to accomplish this objective.

2.2. VHF rain signal from X-band power spectra

Recall that the radar reflectivity, for Rayleigh scatterers, can be expressed as (e.g., Rinehart, 1997):

$$\eta = \frac{\pi^5 |K|^2}{\lambda^4} \frac{Z}{10^{18}}; \quad (3)$$

where $|K|^2$ is the dielectric factor, and λ is the wavelength of the radar transmitted pulse (in meters). Z is the reflectivity factor (expressed in $mm^6\ m^{-3}$). By convention (e.g., Smith 1984), $|K|^2$ is taken equal to 0.93 (the value corresponding to liquid water at near 20ºC, and wavelengths in the S band). Therefore, $Z = Z_e$, the equivalent radar reflectivity factor, is used. This convention is adopted because when radar measurements are made, one is often not certain of the hydrometeor phase or composition.

Therefore, from an original field of Z we can derive a field of η [using (3)], and then apply either (1) or (2) in order to obtain the radar received power. Operationally, on the other hand, the radar will measure received powers, and these will have to be converted into equivalent reflectivity factors. This can be done easily from (1), which is an approximation, but it cannot be done directly if the more realistic equation (2) is used (notice that here η is within the integral).

However, we were able to obtain reflectivity factor values through equation (2) by using the following method. First, a field of Z is input in equation (3) in order to obtain η ($|K|^2 = 0.93$ is used here). Then, we input this reflectivity in (2) to obtain a realistic radar received power (for a given radar range gate). Next, we input the received power from (2) into (1) in order to obtain an

* *Corresponding author address:* Edwin F. Campos, McGill University, Dept. of Atmospheric & Oceanic Sciences, 805 Sherbrooke Street West, Montreal, Quebec, Canada. H3A-2K6; e-mail: ecampos@zephyr.meteo.mcgill.ca .

average (within the radar gate) reflectivity, $\overline{h}$. An average equivalent reflectivity factor (for the radar gate) is then obtained by rearranging (3) as follows:

$$\overline{Z}_e = \frac{l^4\, 10^{18}}{p^5 \left|\mathrm{K}\right|^2} \overline{h} \,. \qquad (4)$$

The procedure is repeated for all the radar range gates. At the end, we were able to estimate the effect of equation (2) by comparing the output $\overline{Z}_e$ and the original Z fields.

For simplicity, we used Z fields that were variable only with height (i.e., one-dimensional fields). Therefore

$$h = h(heigth) = h(r\cos q) \,. \qquad (5)$$

As well, we used for F the values plotted in Figure 1, which come from a simulation of the McGill VHF antenna polar diagram (provided by Mardoc Inc., the builder of this radar). The values in Table 1 were also used, and the antenna effective area was computed from (e.g., Skolnik, 1990)

$$A_e = \frac{D_{\max}\, l^2}{4p} \,. \qquad (6)$$

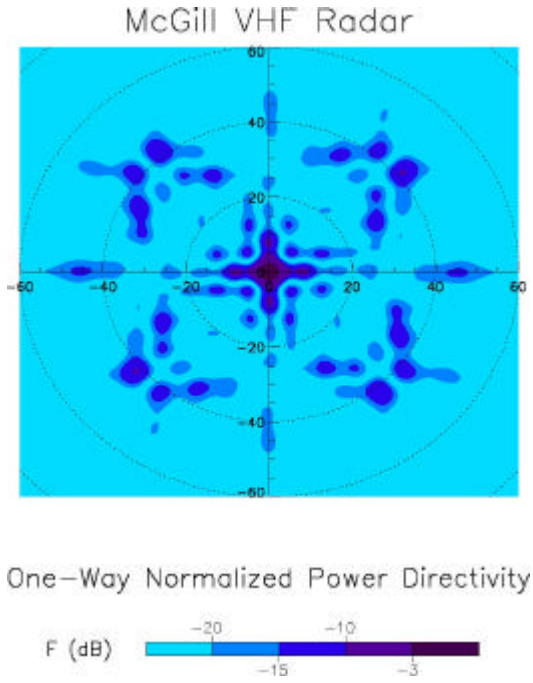

Figure 1. *Antenna pattern of the McGill VHF radar.*

Notice that the integrals in equations (1) and (2) were computed numerically. Therefore, the accuracy of the programs used for integration required some previous testing. (The reason is that computations were very sensitive to the antenna pattern resolution.) Consequently, we first generated a synthetic Z profile that was constant in height, put this profile in equation (3) to obtain ?, input this reflectivity into (2), and solved this equation numerically. In principle, the reflectivities resulting after numerical integration ($\overline{Z}_e$) have to be the same than the input (Z), but it is not so if a too coarse resolution is used for the numerical integration. Therefore, we gradually increased the integration resolution until the output reflectivity equalled the input reflectivity (see red continuous and dashed lines in Figure 4).

After validating the integration programs, we generated two different profiles of reflectivity, and then considered their range variation when computing the $\overline{Z}_e$ values through equation (2), i.e., using the above described method. The first profile was a synthetic reflectivity linearly decreasing with height. The second profile corresponded to a ten-minutes smoothed reflectivity-factor measured by a high-resolution vertically pointing radar (i.e., the McGill VPR, described by Zawadzki, Fabry, and Szyrmer, 2001). The results are presented in Section 3.

Table 1. McGill VHF Radar parameters

Parameter	Value
Tx wavelength (?)	5.77 m
Peak Tx power (P_{Tx})	40 kW
Antenna efficiency (e_a)	0.54
Maximum Directivity (D_{max})	457.3
Transmitted pulse length (L)	1 km

2.3. VHF rain signal from VHF power spectra

The automatic separation of the rain signal from the total VHF received power represents an interesting challenge in terms of radar signal processing. On one side, VHF radar Doppler spectra measured during rain events present clearly separated modes corresponding to the clear air (the slowest) and rain (the fastest) signals. One spectrum example is presented in Figure 2, which corresponds to observations by the McGill VHF radar at a range gate between 2.5 and 3.0 km height (agl, above the ground level). This spectrum has a population of scatterers peaking at 3.5 Hz (i.e., a Doppler velocity of about 10 m/s, typical magnitude for raindrop fall velocities), and a slowest population peaking at – 0.5 Hz (i.e., a Doppler velocity of 1.4 m/s, a typical downdraft for Montreal). In fact, it is not rare to observe rain spectral peaks being as strong (or even higher) than the clear air peak. On the other hand, part of the clear air signal is often overlapped into the rain spectral range.

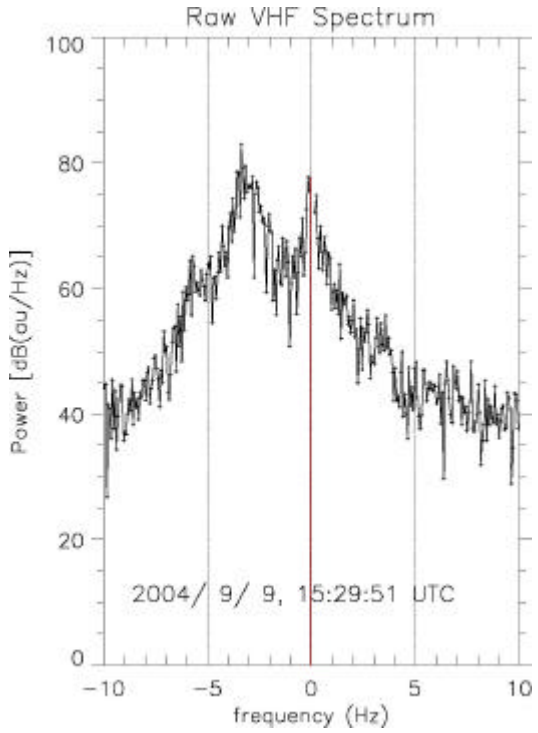

Figure 2. *Doppler power spectrum observed in rain by the McGill VHF radar. For this example, on September 9, 2004, at 15:29:51 UTC, the beam is pointing vertically and the range gate is within 2.5 and 3.0 km. The red vertical line corresponds to the clear-air spectral peak.*

To deal with this challenge, we developed a method for extracting the rain signal out of the total Doppler power spectra, which is valid for any vertically-pointing VHF radars. This method has been developed from an empirical basis (i.e., try and error), and it is described as follows.

We start with the raw spectra (non-calibrated, expressed in arbitrary units, au, per spectral bin) measured by the McGill VHF radar. For a given range gate, a spectrum is obtained every 35 seconds, for a spectral range is within -10.0 and 10.0 Hz, and a spectral bin resolution of 0.067 Hz. Also notice that the ground clutter signal has already been removed by a notch filter at near 0 Hz (see Hocking 1997 for details on the Doppler power spectra derivation). We calibrate these spectra by using a relationship of the form

$$P_{out}\ B_{sky} + A_{sky} = P_{cal}\ ; \qquad (7)$$

where the subscript *out* correspond to the radar raw output, the subscript *cal* corresponds to the calibrated power, and the subscript *sky* corresponds to the values derived from a sky-noise calibration (see Campos et al. 2005, in this issue).

Therefore, the power-densities (S) calibration equation for the i-th spectral bin is given by

$$S_{cal}(f_i) = \frac{1}{n}\frac{A_{sky}}{\Delta f} + B_{sky}\ S_{out}(f_i) \quad . \qquad (8)$$

The second step consists in finding the clear-air spectral peak. To do this, we search for the four largest power density values located into the spectral range between -0.8 and 0.8 Hz (we have noticed that the clear-air peak is usually located here). If these 4 points do not lie within less than 0.81 Hz of each other, then we stop the procedure and conclude that no clear-air signal can be retrieved. Otherwise (if the four points lie within 0.8099…) we compute the average frequency for these points, and the frequency bin for the clear-air peak, f_p, will be the one closer to this average frequency. The red line in Fig. 2 indicates the clear-air peak obtained for this particular case.

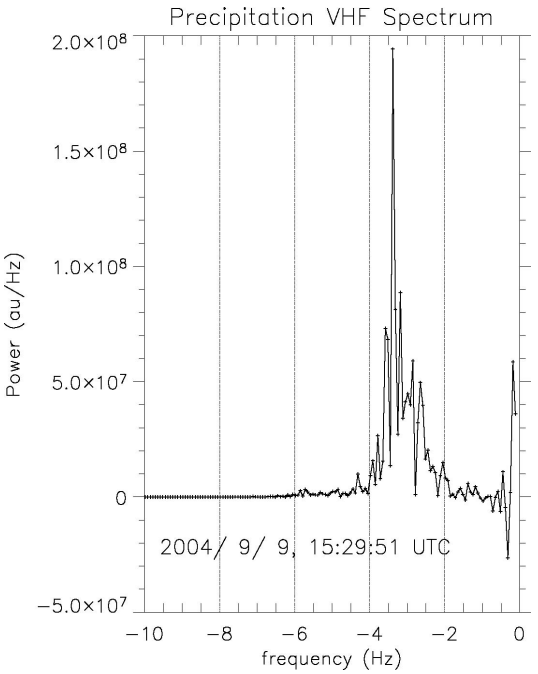

Figure 3. *Precipitation spectrum extracted from the Doppler power spectrum in Fig 2 and eqn. (9).*

During the third step, we subtract the clear air signal to the recorded Doppler power spectrum, and the remaining spectrum will then be the one corresponding to precipitation. We use the fact that the clear-air spectrum is normally distributed; therefore, the clear-air signal at n spectral bins to the right of the clear-air peak should be the same (on average) than at n spectral bins to the left of the clear-air peak. We will not expect to

have precipitation signal to the right of the clear-air peak, but only to the left of this peak (since precipitation Doppler velocities in the vertical are always smaller than eddies Doppler velocities). Therefore, it is safe to assume that the rain power density is given by

$$S_{precip}(f_{j-i}) = S(f_{j-i}) - S(f_{j+i}); \quad (9)$$

where $S_{precip}(f_n)$ is the precipitation Doppler power density at the n-th spectral bin (in Watts per Hz), $S(f_n)$ is the raw Doppler power density at the n-th spectral bin (in Watts per Hz), j is the spectral bin corresponding to the clear-air peak, and i is any given spectral bin.

Figure 3 presents the result of applying eqn. (9) to the Doppler power spectrum in Fig. 2. From multiple observations of the performance of this method with real data, we have estimated that the largest Doppler frequency valid for the rain spectrum is located at 1.0 Hz to the left of the clear-air peak, i.e.,

$$f_{precip} \in [-10.0, (f_j - 1.0)]\ Hz\ . \quad (10)$$

2.4. Dataset requirements

In order to apply the methods described above, VHF radar measurements need to be taken during an event of wide spread precipitation, having a melting level much higher than the lower radar range gate (so that we can guarantee rain measurements at least at the very first range gates). For the McGill VHF radar, the lowest range gate is between 2.5 and 3.0 km height, and it is rare that wide spread precipitation over Montreal presents bright bands above this height. However, we managed to collect a very excellent precipitation event that fulfills these requirements. It corresponds to the passage of the remnants of hurricane Frances over the radar site, on September 9, 2004.

3. RESULTS

The effect of a variable reflectivity field in the radar equation was studied by generating a synthetic profile of reflectivity, where Z decreases logarithmically linear with height (10 dBZ_e per km, the typical value we can observe in snow over Montreal). This Z profile was used as input for obtaining $\overline{Z}_e$ through the method described in the previous section. Figure 4 presents the input Z profile in black dashed line, and the output $\overline{Z}_e$ profile is also plotted in a black continuous line. The results indicate a deepening in the $\overline{Z}_e$ slope with height. A small under estimation (of $\overline{Z}_e$ with respect to the input Z) is observed below the 4km level, and the difference between input and output been greater at higher ranges (reaching 9 dBZ at 9 km).

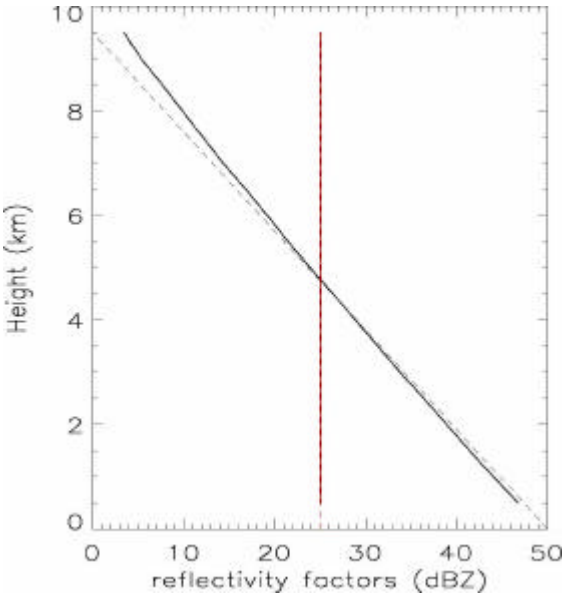

Figure 4. *Examples using synthetic data as input. Red lines correspond to a validation test with input of constant Z. Black lines corresponds to a linearly decreasing profile of Z. Dashed lines are input profiles (Z) and continuous are output profiles ($\overline{Z}_e$).*

A second experiment aimed to present more realistic conditions by using a real profile of reflectivity. For this, height profiles of the equivalent radar reflectivity factor, measured by the McGill VPR, are used. The VPR was co-located with the McGill VHF radar, and its dataset have a time resolution of about 30 seconds and a range resolution of about 75 meters. We smoothed these VPR measurements by taking, for each particular range gate, the 10-minutes median value.

Since the VPR operates at X band, precipitation attenuation has to be considered. We then had to re-calibrate the VPR measurements, and this was done by comparing the equivalent reflectivity factors derived from Drop size distributions (DSDs). The DSD measurements where taken at ground by a Precipitation Occurrence Sensor System (POSS, described by Sheppard, 1990), collocated with the VPR and the VHF radars. For the event on September 9, 2004, a time lag of -1.5 minutes was added to POSS observations. This lag was determined from the lower panel in Figure 5, where the maximum of the cross-correlation function between POSS derived and VPR measured equivalent reflectivity factors is located at zero lag when -1.5 minutes are added to POSS times. The upper panel in Figure 5 presents the time series (after the POSS time lag correction) of simultaneous measurements by POSS (black continuous line) and VPR (red dashed line). The POSS values (Z_{POSS}) correspond to the 10-minutes median at a height of about 2 meters (above ground level, agl), while the VPR values (Z_{VPR}) correspond to the 10-minutes median at 450 meters agl (the lowest range gate). The underestimation (due to attenuation)

by the VPR is clear. Therefore, a VPR calibration factor, which compensates for the rain attenuation at X band, is obtained from

$$Cal.Factor \equiv Median\left[\frac{Z_{POSS}(t_i)}{Z_{VPR}(t_i)}\right] = 26.70 \qquad (11)$$

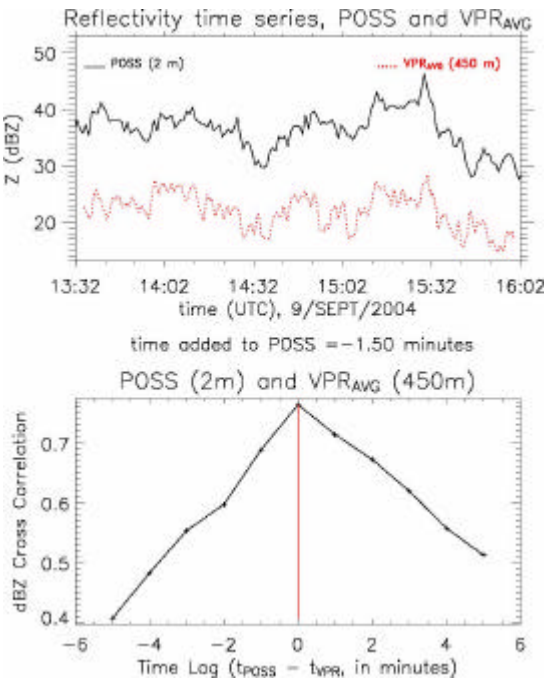

Figure 5. *Lower: Cross-correlation function between POSS and VPR observations. Upper: Radar reflectivity factors simultaneously measured by the McGill VPR radar and the POSS drop size distributions. In both panels, 1.5 minutes have been subtracted to POSS time series.*

Figure 6 the data from the upper panel in Fig.5 as a scatter plot (139 pairs in total). The black line corresponds to the hypothetical case when Z_{POSS} and Z_{VPR} are equal, and the red line corresponds to the case when the calibration factor in (11) is multiplied to Z_{VPR}. Notice how this red line is located in the observations cloud, which validates the use of (11) as attenuation corrector.

The black dashed line in Figure 7 presents the profile of equivalent reflectivity factor measured by the VPR, after all corrections from the previous two paragraphs have been applied. We used this VPR profile as the input Z, for the algorithm described in section 2.2, in order to obtain $\overline{Z}_e$ (plotted as the red histogram-like line). Notice that $\overline{Z}_e$ is in fact a simulation of the VHF Z_e from X band Z_e observations.

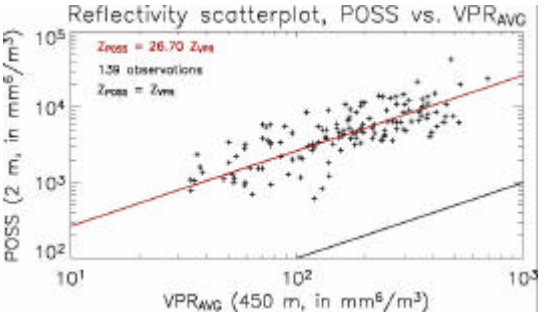

Figure 6. *VPR calibration from POSS DSDs derived Z.*

For comparison, the rain signal measured by the VHF radar is also plotted, as blue lines , in Figure 7. This rain signal was obtained from the method described in section 2.3. For the coefficients in equation (7), we used equation (11.c) by Campos et al. (2005), i.e.,

$$P_{cal} = \left(-1.667x10^{-14} \pm 1.4\times10^{-15}\right)[W] + P_{out}\left(1.695x10^{-20} \pm 5.1\times10^{-22}\right)[W/au] \qquad (12)$$

4. DISCUSSION

From this study, it is found that the space-variable reflectivity has a relevant effect on the radar equation only above the melting level. Above these heights, the side lobes of the antenna polar diagram are collecting enhanced power from scatterers located in the bright-band (i.e., ranges in the side-lobe direction corresponding to bright-band height).

From these results, we also expect that rain-only equivalent reflectivity factors will be about the same at X band than at VHF band (when X band measurements are corrected for attenuation). Therefore, it is valid to use equation (1) for quantitative measurements of rain by VHF radars. However, the expression (2) has to be considered when dealing with snow quantitative measurements at VHF band.

Differences in Z from X and VHF band observations can be due mainly to (a) incorrect radar absolute calibration, (b) $|K|^2$? 0.93, (c) effect of the space-variable reflectivity and antenna sidelobes, (d) inaccurate simulation of the antenna polar diagram F, (e) non-uniformity of the raindrop field observed by the VHF radar (see Fabry, 1996, for implications). As future work, all these sources of error should be explored individually more in detail.

For the single reflectivity profile presented in Fig. 7, the comparison between the simulated and measured VHF rain signals (i.e., red and blue lines in Fig. 7) presents a bias in the order of 14 *dBZ$_e$*. We associate this bias to the values used in equation (12), i.e., the radar calibration. There is, however, good agreement in terms of the shape of VHF reflectivity profiles below the melting level (i.e., below 4.5 km height in Fig. 7). Based on this agreement, this comparison can be used as a calibration method for VHF ST radars, if the VHF radar

observations are expressed in arbitrary units (of the analog-to-digital-converter in the receiver). This new calibration method requires the analysis of more reflectivity profiles, which will be undertaken as future work.

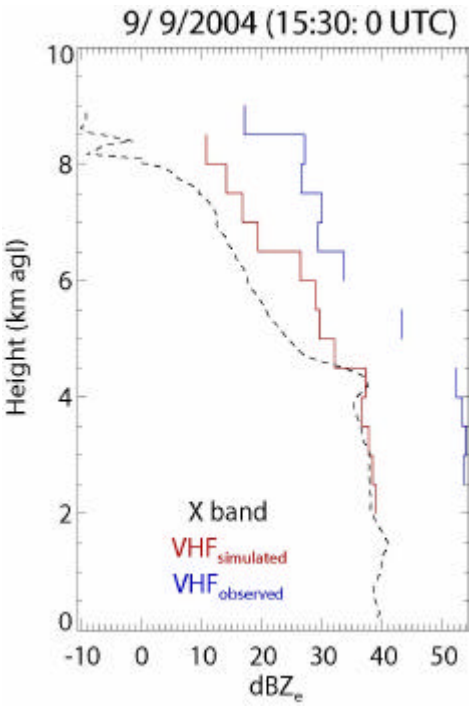

Figure 7. *Simulated VHF Z_e profile (continuous red line) from observed X band Z_e profile (black dashed line). The corresponding VHF observations are plotted as blue lines. Co-located and simultaneous radar observations, at X and VHF bands, were taken on September 9, 2004, at 15:30 UTC.*

References

Campos, E.F., Hocking, W., and Fabry, F., 1997: Power Calibration of VHF Stratospheric-Tropospheric radars. Preprints of the 32nd Conference on Radar Meteorology, Albuquerque, NM, USA, P12R7 in this issue, American Meteorological Society, Boston, MA, USA.

Fabry, F., 1996: On the determination of scale ranges for precipitation fields. *Journal of Geophysical Research*, **101**, D8, 12,819-12,826.

Hocking, W. K., 1997: System design, signal-processing procedures, and preliminary results fro the Canadian (London, Ontario) VHF atmospheric radar, *Radio Science*, *32*(2), 687-706.

Rinehart, R.E., 1997: Radar for Meteorologist, Third Edition. Rinehart Publications, Grand Forks, ND, USA, 428 pp.

Sheppard, B., 1990: Measurement of Raindrop Size Distributions Using a Small Doppler Radar. *Journal of Atmospheric and Oceanic Technology*, **7**, 255-268.

Skolnik, M.I., editor, 1990: *Radar Handbook*, Second Edition. McGraw-Hill. Available on the Internet at *http://www.knovel.com/knovel2/Toc.jsp?BookID=701*.

Smith, P.L., 1984: Equivalent Radar Reflectivity Factors for Snow and Ice Particles. Journal of Climate and Applied Meteorology, **23**, 1258-1260.

Zawadzki, I., Fabry, F., Szyrmer, W., 2001: Observations of supercooled water and secondary ice generation by a vertically pointing X-band Doppler radar. *Atmospheric Research*, **59-60**, 343-359.